19951209 41

N95-27362

TURBULENCE BOUNDARY CONDITIONS FOR SHEAR FLOW ANALYSIS, USING THE DTNS FLOW SOLVER

404941
317-34
45110
p. 16

M. Mizukami
NASA Lewis Research Center
Cleveland, Ohio

SUMMARY

The effects of different turbulence boundary conditions were examined for two classical flows: a turbulent plane free shear layer and a flat plate turbulent boundary layer with zero pressure gradient. The flow solver used was DTNS, an incompressible Reynolds averaged Navier-Stokes solver with k-ε turbulence modeling, developed at the U.S. Navy David Taylor Research Center. Six different combinations of turbulence boundary conditions at the inflow boundary were investigated: In case 1, 'exact' k and ε profiles were used; in case 2, the 'exact' k profile was used, and ε was extrapolated upstream; in case 3, both k and ε were extrapolated; in case 4, the turbulence intensity (I) was 1%, and the turbulent viscosity (μ_t) was equal to the laminar viscosity; in case 5, the 'exact' k profile was used and μ_t was equal to the laminar viscosity; in case 6, the I was 1%, and ε was extrapolated. Comparisons were made with experimental data, direct numerical simulation results, or theoretical predictions, as applicable. Results obtained with DTNS showed that turbulence boundary conditions can have significant impacts on the solutions, especially for the free shear layer.

INTRODUCTION

Turbulent shear flows play a major role in many aerospace and fluid dynamics applications. Wall bounded turbulent shear flows, i.e. turbulent boundary layers (TBL), are present in nearly all moderate to high speed external and internal flows. Turbulent free shear layers (FSL) are important for many applications such as flow mixers and thrust producing nozzles.

In computational fluid dynamic (CFD) analyses, the use of an appropriate boundary condition (BC) is a critical element in assuring convergence to an accurate solution. Use of inappropriate boundary conditions may cause any one or more of the following: inaccurate solutions, poor convergence, nonphysical effects, or divergence.

For turbulent flows, the k-ε turbulence model introduces two new flow properties, turbulent kinetic energy (k) and turbulent dissipation (ε), each with its corresponding transport equation which must be solved numerically by the flow solver. As for any other flow property, it would seem to be essential to assign the proper boundary conditions for k and ε, especially on the inflow boundary, where the flow enters the computational domain. However, the use of appropriate turbulence BC's is frequently underemphasized or neglected.

Ideally, the exact profiles of k and ε would be known, and they would be applied as the inflow BC, but that is usually not feasible. Experimental k profiles are sometimes available, but

often with inadequate resolution for use as a CFD BC, especially near the wall. Measurement of k requires an unsteady measurement of flow velocity, with a response time fast enough to capture the smallest turbulence time scales, preferably in 3 components to take into account turbulence anisotropy. ε is almost impossible to measure experimentally, as it is calculated from the second derivatives of mean flow properties, requiring exceedingly accurate measurements on a very fine survey grid.

Many flow solvers simply extrapolate k and ε on non-wall boundaries of the solution domain. But upstream extrapolation of turbulence properties at the inflow boundary is counter intuitive, and it has been shown to produce inaccurate results (Georgiadis and Yoder 1994). In particular, extrapolation of k and ε at the inflow appeared to inhibit the production of k near the inflow plane, resulting in locally lower turbulent viscosity. Furthermore, the eigenvalues of both k and ε transport equations are equal to the mean flow velocity, indicating that at the inflow boundary, k and ε values should be specified (Hirsch 1990).

Alternately, some turbulence properties could be assigned uniform values over the entire inflow boundary. Uniform turbulence intensity (I) and turbulent viscosity (μ_t) could be specified; k and ε values, which will vary across the boundary depending on the mean flow properties, can be derived from I and μ_t. Another possibility is to specify uniform I and turbulent length scale (L), and from these derive k and ε. However, the specified values of I and μ_t are typically arbitrary estimates. Georgiadis, Chitsomboon and Zhu (1994) examined a 2-D ejector nozzle, which includes both wall bounded and free shear flows. Specifying uniform I and μ_t at the inflow was found to match the data better than specifying I and L, or extrapolating k and ε.

In the present work, the effects of different CFD turbulence BC's are examined for two classical flows: a turbulent plane free shear layer and a flat plate turbulent boundary layer with zero pressure gradient. The flow solver used is DTNS, an incompressible Reynolds averaged Navier-Stokes solver with k-ε turbulence modeling. Different combinations of the following boundary conditions are used: 'exact' k profiles, 'exact' ε profiles, extrapolated k, extrapolated ε, uniform I, and uniform μ_t. Comparisons are made with experimental data, direct numerical simulation results, and theoretical predictions, as applicable.

METHODS

Flow Solver

DTNS is an incompressible Reynolds averaged Navier-Stokes flow solver with k-ε turbulence modeling, developed at the U.S. Navy David Taylor Research Center, primarily by Gorski (1988a, 1988b). The three versions of the code are designed to solve two dimensional (DTNS2D), axisymmetric (DTAXI) and three dimensional (DTNS3D) flows, respectively. Although the flows examined herein are two-dimensional, the three dimensional flow solver (DTNS3D) was used here, on a three dimensional grid with 5 identical grid planes in the cross stream direction, so that in the future, methods developed here could be be directly applied to three-dimensional problems of interest.

DTNS was selected for this study for two reasons. First, it is a relatively well established, general-purpose code, with a number of documented test cases with experimental comparisons, such as: cascades (Gorski 1988b), flow over a cylinder (Gorski 1988a), an NACA 0012 airfoil (Gorski 1988a), flow over a backward facing step (Gorski 1988a, Steffen 1992 & 1993) and

laminar boundary layers (Steffen 1992). This allows the present study to focus on the fluid dynamics, instead of the code development and validation. Second, it is an 'open' code, with the source code available. This allows the specialized turbulence BC's to be implemented by modifying the code. In addition, study of the source code leads to a deeper understanding of the computational procedure and the relevance of the resulting solution, which are essential to a fundamental study such as this.

The method of pseudo compressibility is used in the governing equations, so that state of the art schemes developed for compressible flows may be applied to incompressible flows. The total variation diminishing (TVD) scheme of Chakravarthy and Osher is used to discretize the convective terms of the governing equations. The discretized equations are solved implicitly using an approximate factorization method. Gorski (1988a) provides further details on the solution procedure.

The Launder and Spalding (1974) turbulence model is implemented, which is generally considered the standard high Reynolds (Re) number k-ε turbulence model. A wall function model is used, which does not require boundary layers to be resolved using large numbers of packed grid points, thus allowing complex wall bounded flows to be solved with a reasonable number of grid points, and in a reasonable amount of time. Although the profile of an attached turbulent boundary layer is assumed at the wall, the solutions have been found to be accurate even for some drastically separated flows (Steffen 1993). Even low Re k-ε models which resolve the boundary layer in detail on a fine grid, make certain empirical assumptions about the wall bounded flow characteristics. Furthermore, low Re k-ε models models are often highly grid sensitive, and can require extremely finely resolved grids packed very close to the wall to produce an accurate solution (Avva et al. 1990).

The boundary condition routines were modified to allow for different inflow conditions as follows. Mean flow velocities (**u**) are read in from a data file. k and ε may be independently specified at the boundary in two different ways: the profile may be read in from a data file, or it may be zeroeth-order extrapolated. μ_t is calculated from k and ε.

For both the wall bounded and free shear flow cases, six different combinations of k and ε BC's at the inflow boundary were investigated, as shown in table 1. In case 1, 'exact' k and ε profiles are used. In case 2, the 'exact' k profile is used, and ε is extrapolated upstream. In case 3, both k and ε are extrapolated; this is the default case for DTNS. In case 4, the I is uniformly 1%, and μ_t is equal to the laminar viscosity; k and ε values are derived from these using the following expressions. k and I are related by:

$$k = \frac{3}{2} I^2 \|\mathbf{u}\|^2 \tag{1}$$

In this turbulence model ε and μ_t are related by:

$$\mu_t = C_\mu \rho k^2 / \varepsilon \tag{2}$$

where C_μ=0.09, and the damping terms are neglected. In case 5, the 'exact' k profile is used, μ_t is equal to the laminar viscosity, and ε is calculated from (2). In case 6, the I is 1%, k is derived from I as in (1), and ε is extrapolated.

The amount of detailed turbulence information required at the inflow boundary varies from case to case. Case 1 requires both k and ε profiles; this is the most ideal case, but as discussed before, ε profiles are almost never available. Cases 2 and 5 require only k profiles; this is typically more feasible than case 1, because turbulence levels, and thus k, are often measured

experimentally. Cases 3, 4 and 6 require no detailed turbulence information at all.

Flat Plate Turbulent Boundary Layer

The flat plate TBL with zero pressure gradient is a fundamental fluid dynamic problem that has been extensively studied. Initial boundary layer flow property profiles are applied at the inflow boundary of the computational domain, the flow is propagated downstream, and the flow at a downstream station is compared with benchmark results. (figure 1)

The direct numerical simulation (DNS, not to be confused with DTNS) results of Spalart (1988) are used to provide the 'exact' inflow conditions at Re_θ = 300, and the benchmark downstream solution at Re_θ = 1410, where Re_θ is the Reynolds number based on the momentum thickness of the boundary layer and freestream velocity. When properly used, DNS is thought to be as accurate as experimental results, and it provides completely detailed information of the flowfield, including information needed to calculate k and ε, which are difficult to measure experimentally.

The grid dimensions are 100 in the streamwise direction, 40 in the vertical direction, and 5 identical planes in the cross flow direction to accommodate the 3D flow solver. The grid is packed to the wall such that at the inflow boundary y^+ is about 20. The bottom wall has a no slip boundary condition, the top 'far' wall is a slip wall, the sides are slip walls, and the outflow has a constant pressure. Convergence was typically obtained in several thousand iterations, depending on the particular case.

Turbulent Plane Free Shear Layer

The turbulent plane FSL is one of the simplest free shear layers, and it too has been extensively studied. The computational domain consists of the free shear layer mixing region only, with the upstream boundary at the trailing edge (TE) of the splitter plate (figure 6). As in the TBL, the initial profiles are applied at the upstream BC of the computational domain, the flow is propagated downstream, and the flow at a downstream station is compared with exact results.

The plane free shear layer in the McCormick's (1993) experiment is simulated, and comparisons are made with data from the extensive flow diagnostics in the mixing region. McCormick's facility consists of a fan driven wind tunnel, a contoured splitter plate, screens on one side to slow the flow, and a square test section. The flow velocity on the slower, upper side (U_1) is 4.88 m/s, and the velocity on the faster, lower side (U_2) is 8.53 m/s, giving a velocity ratio of 1 : 1.75. Just upstream splitter TE, the momentum thickness (θ) is 1.237mm on the upper / low speed side, and θ = 1.107mm on the lower / high speed side. Extensive measurements were made with triple sensor hot film probes of all three velocity components, including turbulence properties. The flow was visualized using smoke injection and laser light sheets.

The 'exact' u, k and ε profiles at the upstream boundary of the computational domain (i.e. at the splitter TE) were obtained from a separate DTNS solution to a flat plate TBL, because k and ε profiles at the splitter trailing edge were not measured experimentally. Certainly, the resulting solution of the FSL will be affected by the accuracy of the DTNS TBL solutions, but they should be sufficiently accurate for purposes of comparing with other substantially different k and ε BC's. The DNS TBL solutions discussed above could not be used for this purpose, because the Re_θ values do not correspond to those at the splitter TE.

The grid dimensions are 60 in the streamwise direction, 39 across the shear layer, and 5

identical planes in the cross flow direction to accommodate the 3D flow solver. The grid is packed such that y^+ is between 20 and 30 at the inflow boundary. The sides are slip walls, and the outflow has a constant pressure. Convergence was again typically obtained in several thousand iterations, depending on the particular case.

RESULTS

Flat Plate Turbulent Boundary Layer

Figure 2. shows the downstream development of the boundary layer momentum thicknesses (θ) for the six cases, and the TBL 1/5th power law approximate theory predictions (Kuethe & Chow 1986). Downstream distance is nondimensionalized as the Reynolds number based on the distance from the upstream plane (ΔRe_x). Cases 2 and 3 show good agreement with theory. In cases 4, 5 and 6, boundary layer development near the inflow boundary is suppressed. Surprisingly, case 1, the ideal case with all turbulence properties exactly specified, also shows slightly suppressed boundary layer development near the inflow boundary. However, downstream of the initial discrepancies, all 6 cases quickly approach the same theoretical slope.

At the inflow boundary, $\Delta Re_x = 0$ and $\Delta Re_\theta = 300$. Comparisons of u, k and ε profiles are made downstream at the $\Delta Re_x = 551000$ plane, where the approximate theory predicts that $\Delta Re_\theta = 1410$.

Figure 3a shows the 'exact' u profile, specified at the inflow boundary in all 6 cases. Figure 3b shows the u profile at the downstream plane. Although the profiles have slightly different in thicknesses, all have the about the same shape as the DNS solution.

Figure 4a show: the 'exact' inflow k profile used in cases 1,2 and 5; the k profile for I=1% used in cases 4 and 6, which is barely visible next to the vertical axis; and the k profile resulting from upstream extrapolation in case 3. Clearly, $I = 1\%$ specifies k to be much lower than it should be, and upstream extrapolation results in a k that is too high. Figure 4b shows the downstream k profiles. Despite the drastically different initial conditions, all 6 cases match the DNS solution shape surprisingly well, but again with slightly different thicknesses.

Figure 5a shows the exact ε profile used in case 1, the profiles specified in cases 4 and 5, and the profiles resulting from upstream extrapolation in cases 2, 3 and 6. Case 3, with both k and ε extrapolated upstream, gives the best prediction of the initial ε profile after case 1, but this is most likely a fortunate coincidence. Cases 2 and 6 results in ε profiles that are too low. Case 5 specifies an ε profile that is too high. The case 4 profile is not visible on the graph, because, the ε values are all near zero. Figure 5b shows the downstream ε profiles. All 6 cases fall on approximately the same curve, and overpredict ε.

Turbulent Plane Free Shear Layer

Figure 7. shows the downstream development of the shear layer momentum thicknesses (θ) for the six cases. θ is indicative of the amount of mixing taken place between the high and low speed flows, and is defined as:

$$\theta = \int \frac{(u - U_2)(U_1 - u)}{(U_2 - U_1)^2} dy \tag{3}$$

where U_1 is the mean velocity of the upper / low speed side, and U_2 is the velocity of the bottom / high speed side.

Downstream distance is nondimensionalized as the Reynolds number based on U_1 and the axial distance from the computational inflow plane (Re_x), which coincides with the trailing edge (TE) of the splitter plate. Note that near the splitter TE, θ is actually negative, due to the low speed flow from the splitter boundary layers. Cases 1, 2 and 4 show good agreement with the experimental results of McCormick & Bennett. In cases 5 and 6, shear layer development near the inflow boundary is suppressed. In case 3, the shear layer expands at an unrealistically high rate. However, the initial discrepancies in all cases except 6 do not persist far downstream, and the curves shortly approach the same slope.

Profiles of u, k and ε are plotted at three stations: $Re_x = 0$, at the splitter TE and inflow boundary; $Re_x = 28244$, and $Re_x = 290510$. The experimental data for u and k are available and plotted for the two downstream stations for comparisons.

Figure 8a shows the 'exact' u profile, used as the inflow BC in all 6 cases. Figure 8b shows the u profiles at the two downstream stations. At $Re_x = 28244$, cases 4, 5 and 6 appear to give the best agreement with data; at $Re_x = 290510$, cases 1 and 2 appear better. In case 3, the shear layer is far too thick.

Figure 9a show: the 'exact' inflow k profiles used in cases 1, 2 and 5; the k profile for I = 1% used in cases 4 and 6 which is too low to be visible on the plot; and the k profile that results from upstream extrapolation in case 3. Again, I=1% specifies k to be much lower than it should be, and upstream extrapolation results in k that is much too high. Figure 9b shows the downstream k profiles. At both stations, cases 1 and 2 give the best agreement with data, cases 4,5 and 6 underpredict k to varying extents, and case 3 drastically overpredicts k.

Figure 10a shows the 'exact' inflow ε profile used in case 1, the profiles specified in cases 4 and 5, and the profiles resulting from upstream extrapolation in cases 2, 3 and 6. Case 2 underpredicts ε, case 3 creates an unrealistically wide profile, cases 4 and 6 are close to zero and not visible on the plot, and case 5 specifies an unreasonably high spike. Downstream, since no experimental data is available for ε, it is difficult to tell which results are the most accurate, but clearly, the case 3 profile is too wide.

CONCLUSIONS

The effects of different turbulence property CFD boundary conditions were examined using the DTNS flow solver for two classical flows: a turbulent plane free shear layer (FSL) and a flat plate turbulent boundary layer (TBL) with zero pressure gradient. Six different combinations of turbulence property boundary conditions at the inflow boundary were investigated. The major observations and conclusions of the study were as follows:

1. Wall bounded turbulent shear flows appeared to be relatively insensitive to the turbulence inflow BC. Despite drastically different k and ε profiles at the inflow boundary, the mean velocity (u), k and ε profiles downstream were nearly identical, and all cases approached the same correct slope for momentum thickness development. In the near field of the

inflow boundary, cases 1, 4, 5 and 6 suppressed the boundary layer development to varying extents. Cases 2 and 3 gave the best results. Discrepancies in the initial boundary layer development slightly affected the thicknesses at downstream stations.

2. Turbulent free shear flows appear to be more sensitive to turbulence inflow BCs than the wall bounded flows. For free shear flows, all cases except 3 gave reasonably good results, but with more discrepancies between the cases than for wall bounded flows. Cases 1 and 2 gave the best results. Case 5 inhibited the initial shear layer growth, and created an unrealistic spike in the ε profile at the inflow.

3. For free shear flows, case 3 (upstream extrapolation of k and ε at the inflow boundary) gave a drastically high shear layer growth rate. Note that this is the default case for many flow solvers.

4. Overall, when both 'exact' k and ε profiles were used, cases 1 and 2 gave the best results. When only k profiles were used, case 2 was best. When no 'exact' turbulence profiles were used, cases 4 and 6 gave reasonable results.

5. Some additional factors not considered in this study were: compressibility, specifying different levels of uniform turbulence intensity, specifying different levels of uniform turbulent viscosity, and more complex flowfields.

6. The particulars of these findings may vary for different k -ε turbulence models and numerical schemes. However, it is conjectured that overall 'lessons learned' from this study are probably applicable to other flow solvers as well.

REFERENCES

Avva, R., Smith, C. and Singhal, A. Comparative study of high and low Reynolds number versions of k-ε models. AIAA 90-0246

Georgiadis, N. J., Chitsomboon, T. and Zhu, J. 1994 Modification of the two-equation turbulence model in NPARC to a Chien low Reynolds number k-ε formulation. NASA TM to be published.

Georgiadis, N. J. and Yoder, D. A. 1994 Use of Navier-Stokes methods for the calculation of high-speed nozzle flow fields. NASA TM 106551, AIAA 94-3212.

Gorski, J. J. 1988a TVD solution of the incompressible Navier-Stokes equation with an implicit multigrid scheme. in *Proceedings of the AIAA/ASME/SIAM/APS 1st National Fluid Dynamics Congress*, vol. 1, pp. 394-401.

Gorski, J. J. 1988b Incompressible cascade calculations using an upwind differenced TVD scheme. in *Advances and Applications in Computational Fluid Dynamics* (O. Baysal, ed.). ASME-FED. vol. 66, pp. 61-69.

Hirsch, C. 1990 *Numerical Computation of Internal and External Flows, Vol. 2: Computational Methods for Invscid and Viscous Flows*. pp. 344-357. John Wiley & Sons, Chichester.

Kuethe, A. M., and Chow C-Y. 1986 *Foundations of Aerodynamics*, pp. 403-408. John Wiley & Sons, New York.

Launder, B. E. and Spalding, D. B. 1974 The numerical computation of turbulent flows. *Computer Methods in Applied Mechanics and Engineering*. vol. 3, pp. 269-289.

McCormick, D. C. and Bennett, J. C. 1993 Vortical and turbulent structure of a lobed mixer free-shear layer. AIAA 93-0219.

Spalart, P. R. 1988 Direct simulation of a turbulent boundary layer up to $R_\theta = 1410$. *J. Fluid Mech.* **187**, 61-98.

Steffen, C. J. 1992 An investigation of DTNS2D for use as an incompressible turbulence modeling test-bed. NASA TM-105593.

Steffen, C. J. 1993 A critical comparison of several low Reynolds number k-ε turbulence models for flow over a backward-facing step. NASA TM-106173, AIAA 93-1927.

Steffen, C. J. private communications

Table 1. Turbulence property boundary conditions

Case #	k	ε	I	μ_t
1	exact	exact	-	-
2	exact	extrapolated	-	-
3	extrapolated	extrapolated	-	-
4	calc. from I, **u**	calc. from k, μ_t	1%	μ_{lamin}
5	exact	calc. from k, μ_t	-	μ_{lamin}
6	calc. from I, **u**	extrapolated	1%	-

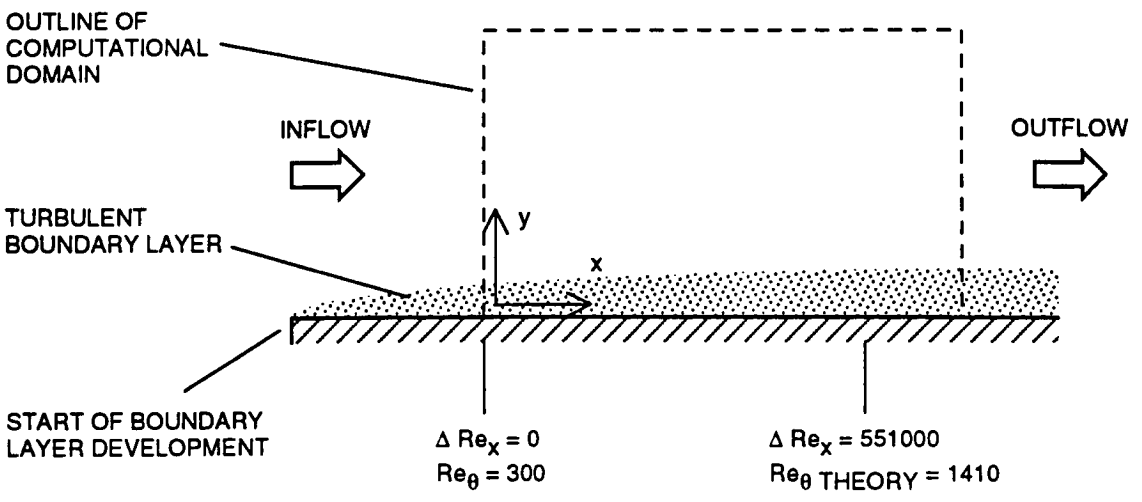

Figure 1. schematic of flat plate turbulent boundary layer (TBL) flow, and computational domain

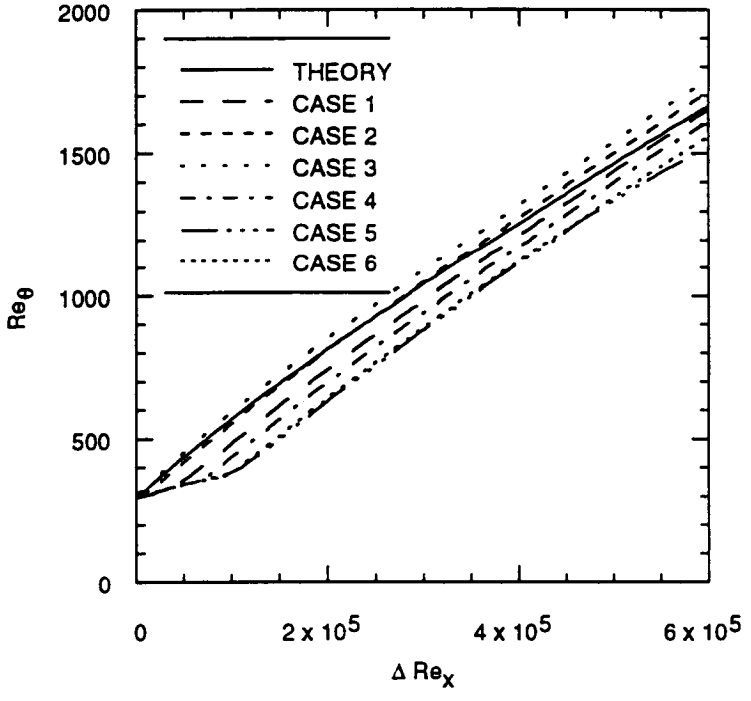

Figure 2. TBL momentum thickness development

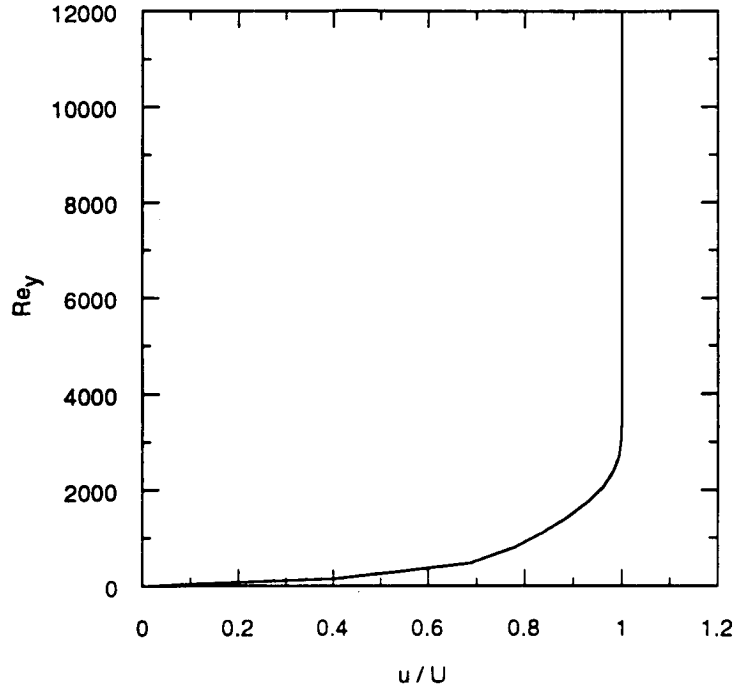

Figure 3a. TBL mean axial velocity profile at inflow boundary ($Re_\theta = 300$, $\Delta Re_x = 0$)

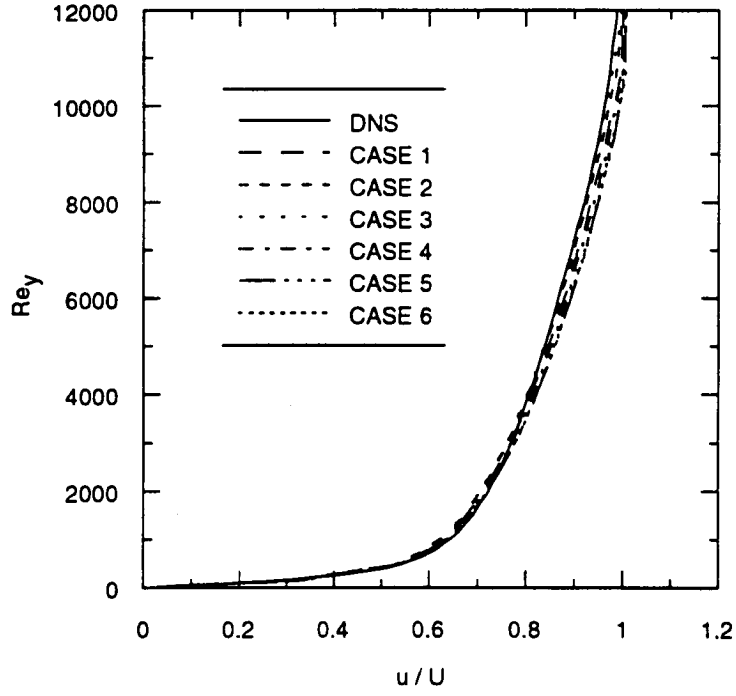

Figure 3b. TBL mean axial velocity profiles at $\Delta Re_x = 551000$

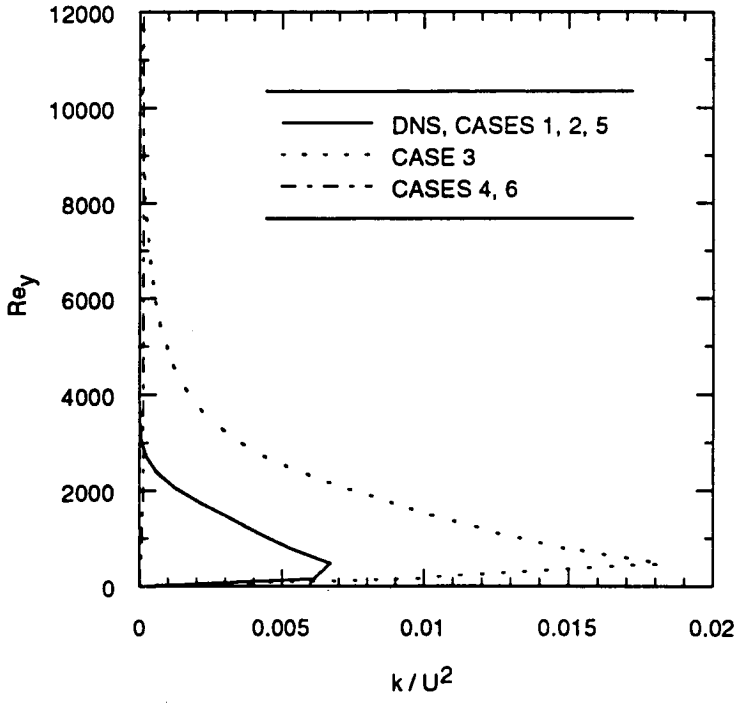

Figure 4a. TBL turbulent kinetic energy profiles at inflow boundary ($\Delta Re_x = 0$)

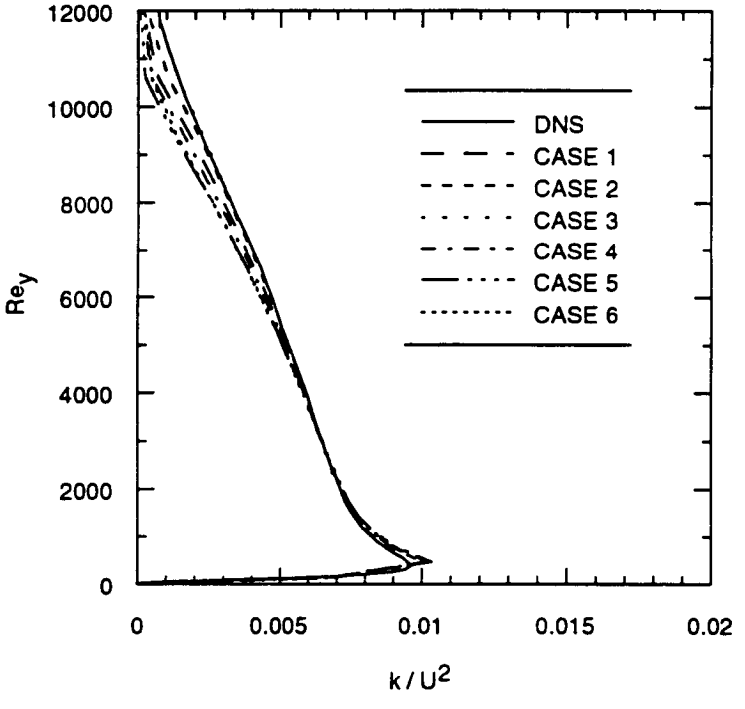

Figure 4b. TBL turbulent kinetic energy profiles at $\Delta Re_x = 551000$

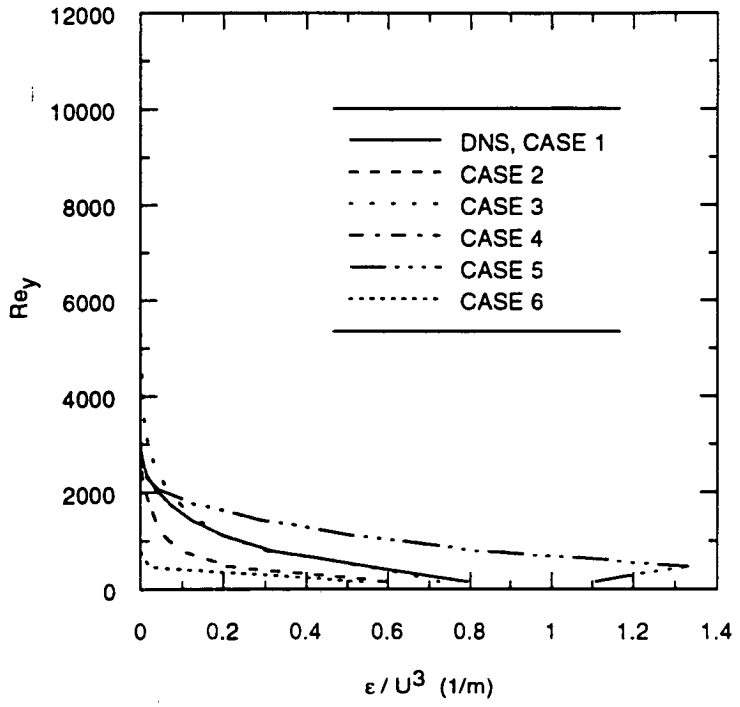

Figure 5a. TBL dissipation profiles at inflow boundary ($\Delta Re_x = 0$)

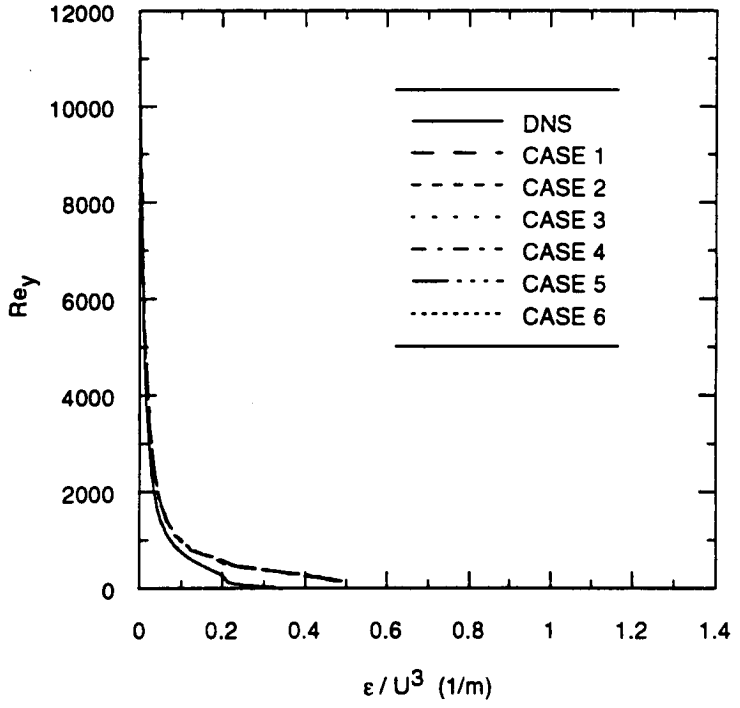

Figure 5b. TBL dissipation profiles at $\Delta Re_x = 551000$

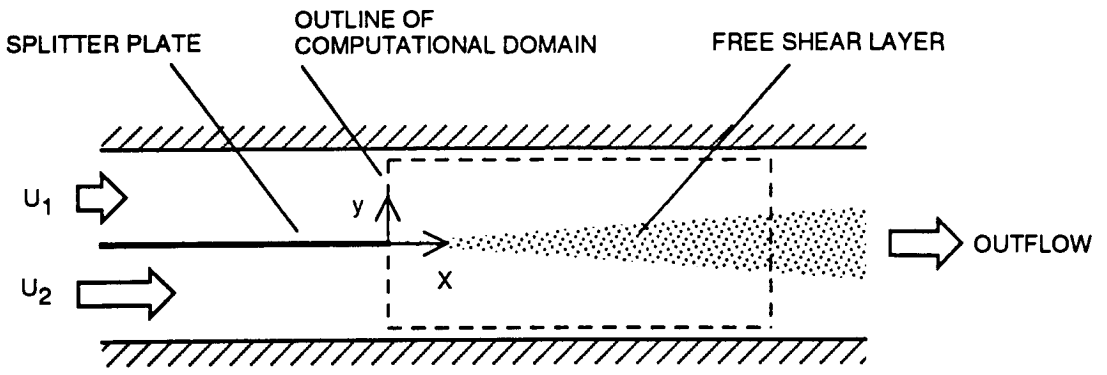

Figure 6. schematic of turbulent plane free shear layer (FSL) flow and computational domain

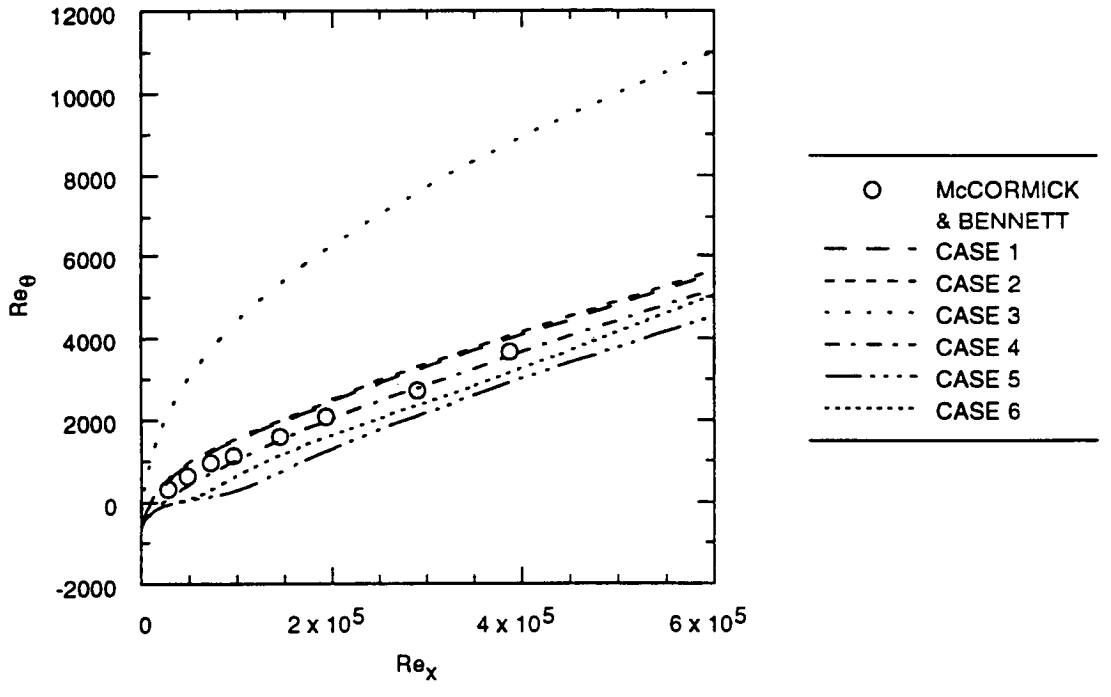

Figure 7. FSL momentum thickness development

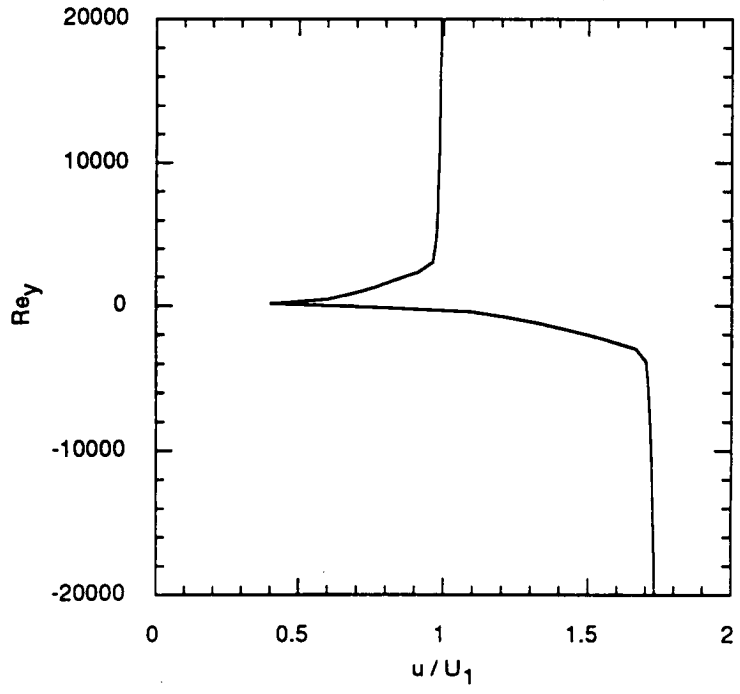

Figure 8a. FSL mean axial velocity profile at inflow boundary ($Re_x = 0$)

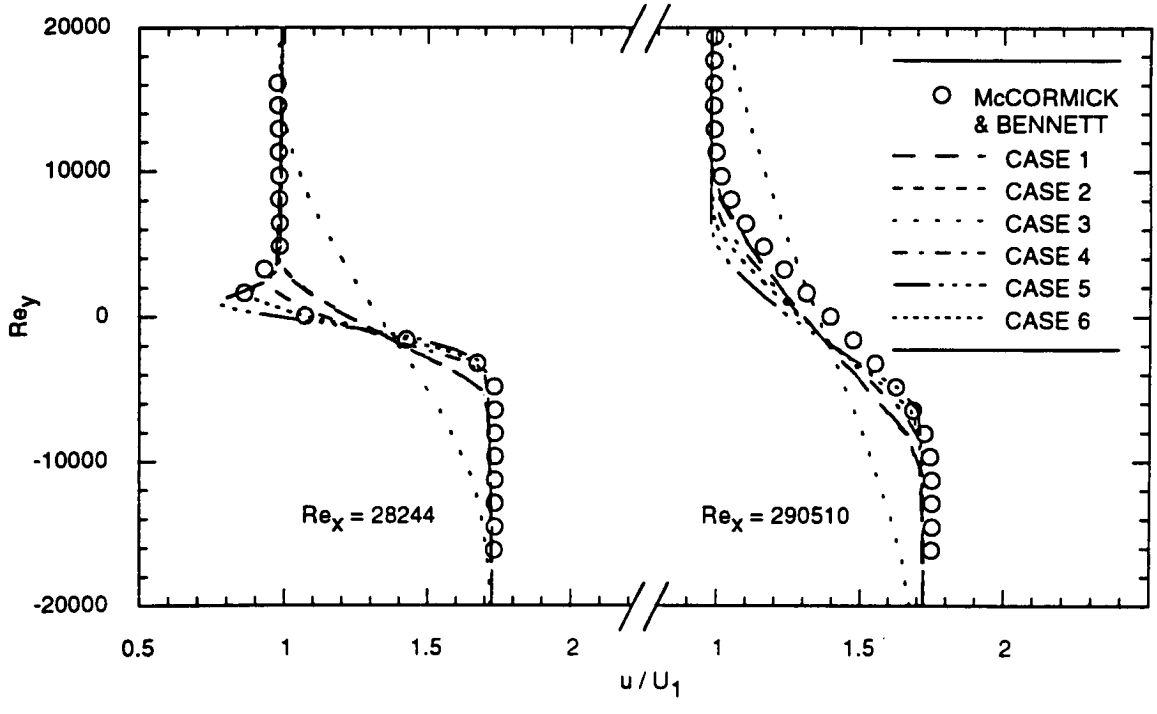

Figure 8b. FSL mean axial velocity profiles at downstream stations

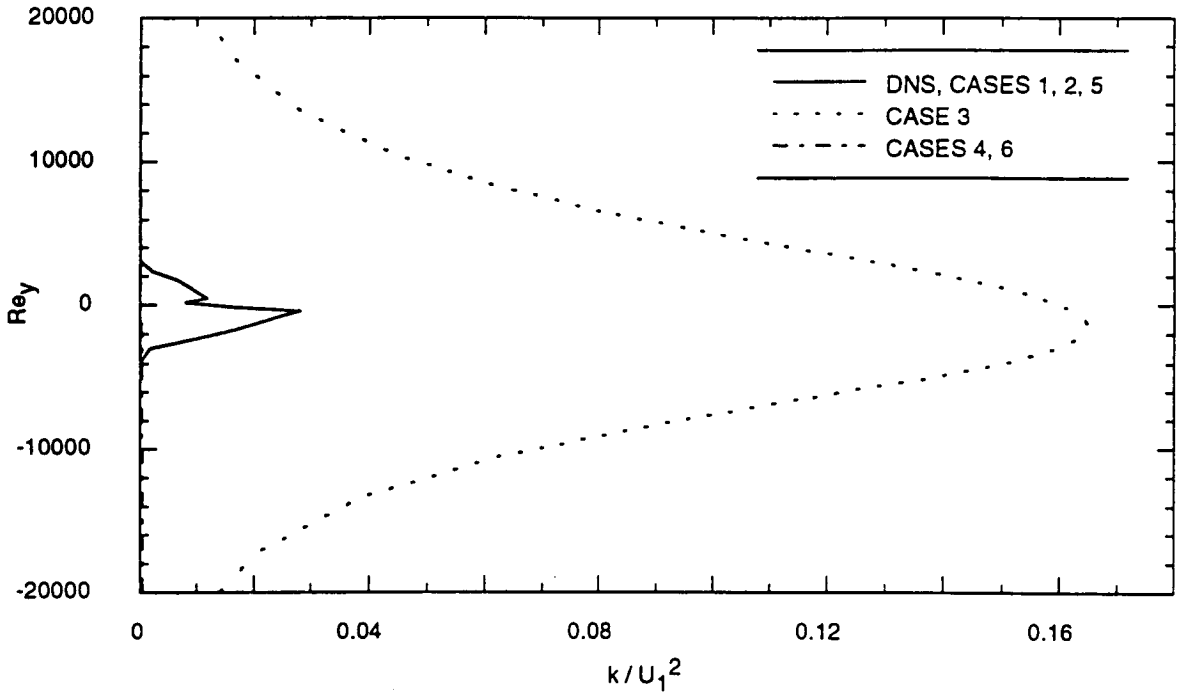

Figure 9a. FSL turbulent kinetic energy profiles at inflow boundary ($Re_x = 0$)

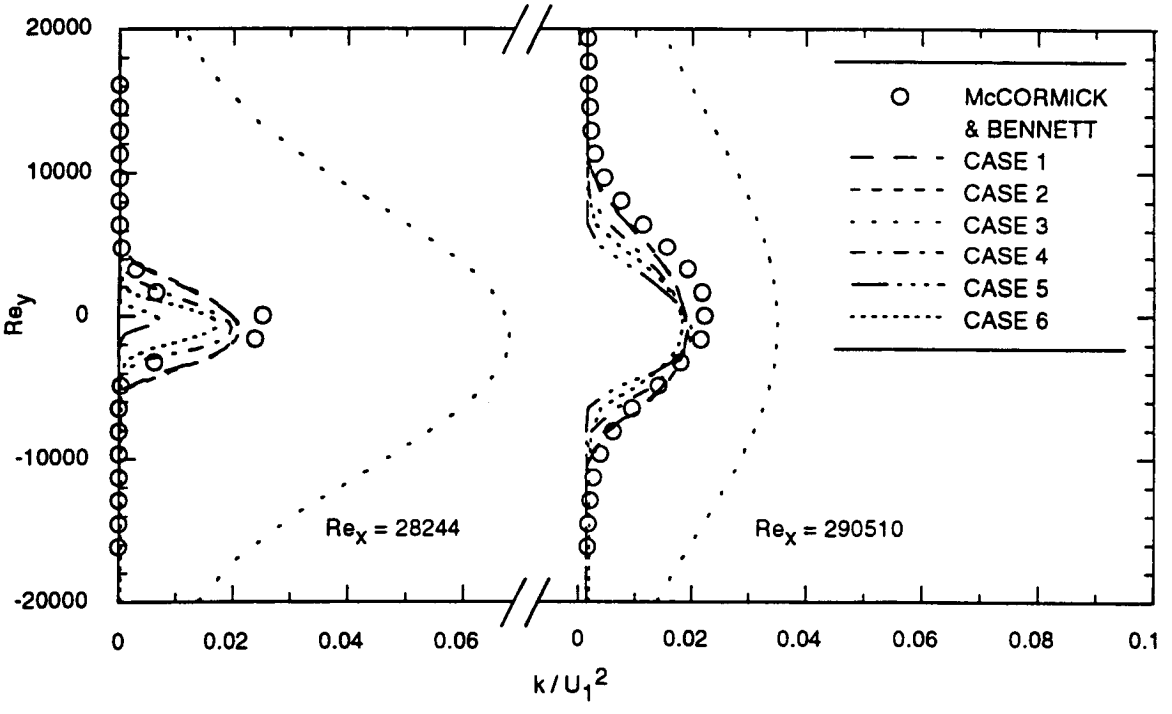

Figure 9b. FSL turbulent kinetic energy profiles at downstream stations

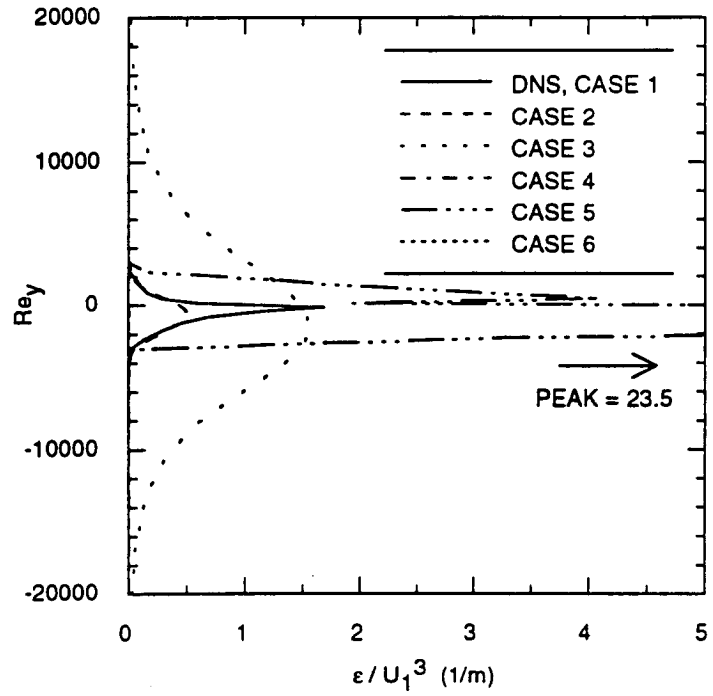

Figure 10a. FSL dissipation profiles at inflow boundary ($Re_x = 0$)

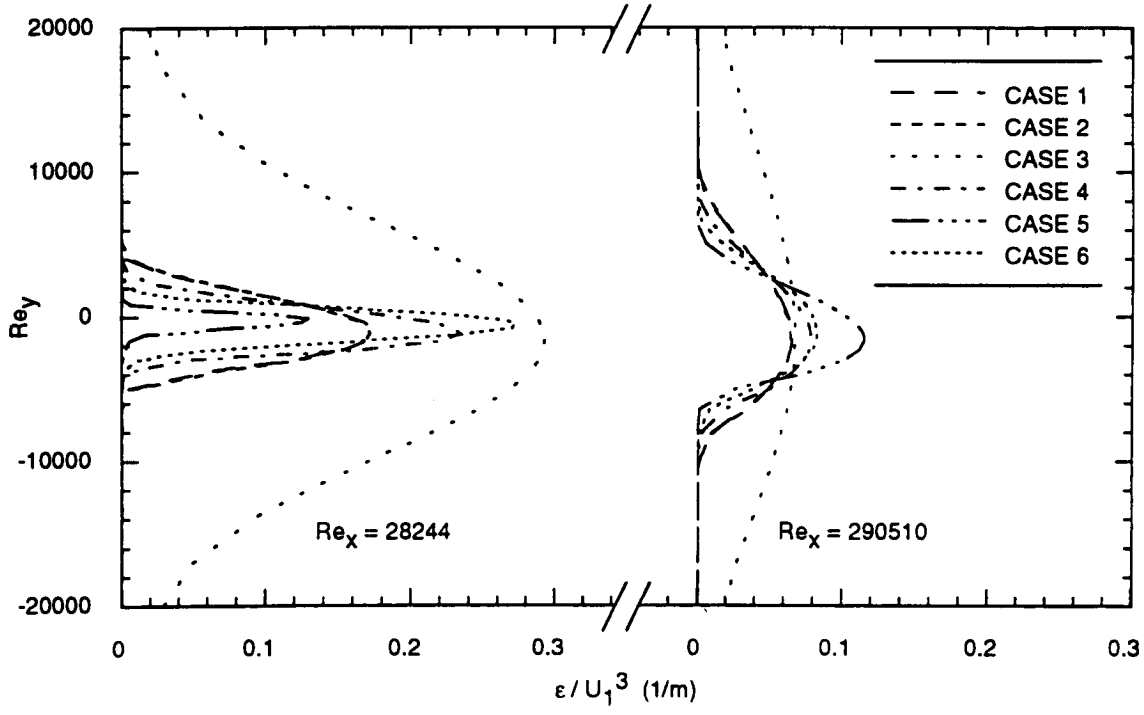

Figure 10b. FSL dissipation profiles at downstream stations